ACS Catalysis

Research Article

pubs.acs.org/acscatalysis

Protonation-Triggered Carbon-Chain Elongation in Geranyl Pyrophosphate Synthase (GPPS)

Jingwei Zhou,[†] Xiaoming Wang,[‡] Ming Kuang,[§] Laiyou Wang,[§] Hai-Bin Luo,[†] Yirong Mo,*[,∥] and Ruibo Wu*[,†]

[†]School of Pharmaceutical Sciences, Sun Yat-sen University, Guangzhou 510006, P.R. China

[‡]Program in Public Health, College of Healthy Sciences, University of California—Irvine, Irvine, California 92697,United States

[§]Institute of Chinese Medical Sciences, Guangdong Pharmaceutical University, Guangzhou 510006, P.R. China

[∥]Department of Chemistry, Western Michigan University, Kalamazoo, Michigan 49008, United States

Supporting Information

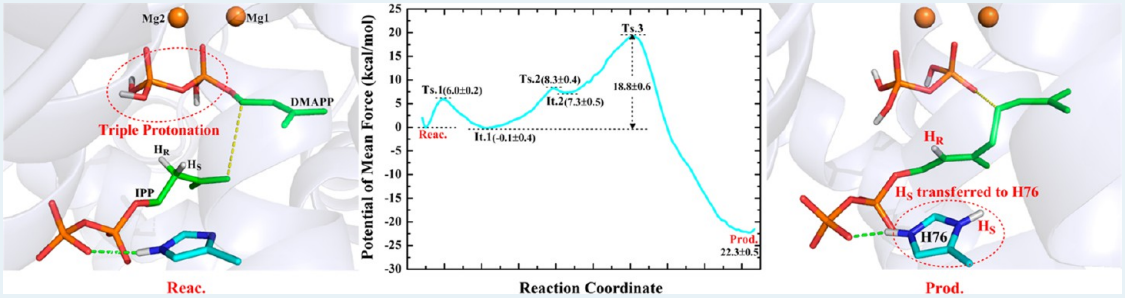

ABSTRACT: Geranyl pyrophosphate synthase (GPPS) is responsible for the formation of geranyl pyrophosphate (GPP), a key intermediate which has the potential to derive numerous functionally and structurally diverse groups of terpenoid natural products via the head-to-tail assembly of two isoprenoid building blocks (dimethylallyl diphosphate, DMAPP; isopentenyl diphosphate, IPP) in the initial step of carbon-chain elongation during isoprenoid biosynthesis. Elucidating the detailed catalytic mechanism in GPPS is of significant interests as it will stimulate the development of new technology in generating novel natural productlike scaffolds. It has been known that the catalytic reaction involves three sequential steps, namely "ionization−condensation−elimination", but the exact catalytic mechanism has remained controversial since the 1970s. By employing Born−Oppenheimer density functional quantum mechanics (B3LYP/6-31(+)G*)/molecular mechanics dynamics simulations, here we suggest that GPPS adopts a protonation-induced catalytic mechanism, in which there are two key points different from previously hypothesized mechanisms. The first point is the protonation of DMAPP which is essential in the initial "ionization" process but was not considered in previous mechanisms. The second point is the stereoselectivity of proton transfer (H_S) from IPP to H76 residue in the final "elimination" step as identified in our simulations, in contrast to the proton transfer from IPP (H_R) to DMAPP in previous hypotheses. Moreover, the free energy barrier of the whole assembly reaction is predicted to be 18.8 ± 0.6 kcal/mol, in agreement with the experimental value of 18.0 kcal/mol. Furthermore, the catalytic roles of the two Mg^{2+} ions at the bottom of the active site are also discussed, and key residues (K44, R47, R94, R95, K180, K235, and E73 around DMAPP and IPP) responsible for the stabilization of transition states, intermediates, and/or product are clarified. These findings can assist site-directed mutagenesis experiments in protein engineering as well as inhibitor designs.

KEYWORDS: *GPPS, catalytic mechanism, assembly, protonation, isoprenoid biosynthesis*

1. INTRODUCTION

As one of the most ancient and widespread classes of structurally and functionally rich biomolecules, the terpene family includes many kinds of compounds that play essential roles in a variety of important biological pathways.[1−4] Almost all terpenes are derived from the universal isoprenoid building blocks, dimethylallyl diphosphate (DMAPP) and isopentenyl diphosphate (IPP).[3−6] As shown in Figure 1, the terpene biosynthetic pathway involves three stages. At the first stage, DMAPP and IPP are synthesized via the mevalonate phosphate pathway (MVA)[4,7−10] or the methylerythritol phosphate pathway (MEP).[4,7,11] Afterward, the synthesized DMAPP grows by further assembling IPP through elongation reactions to form linear or branched hydrocarbon products with longer chains,[12−14] in which enzymes prenyl transferases (PTs) play the catalytic role.[15,16] Finally, the hydrocarbon products would generate a vast assortment of terpene end products by multistep cascade reactions such as rearrangement and/or

Received: December 23, 2014
Revised: June 8, 2015
Published: June 15, 2015

DOI: 10.1021/acscatal.5b00947
ACS Catal. 2015, 5, 4466−4478

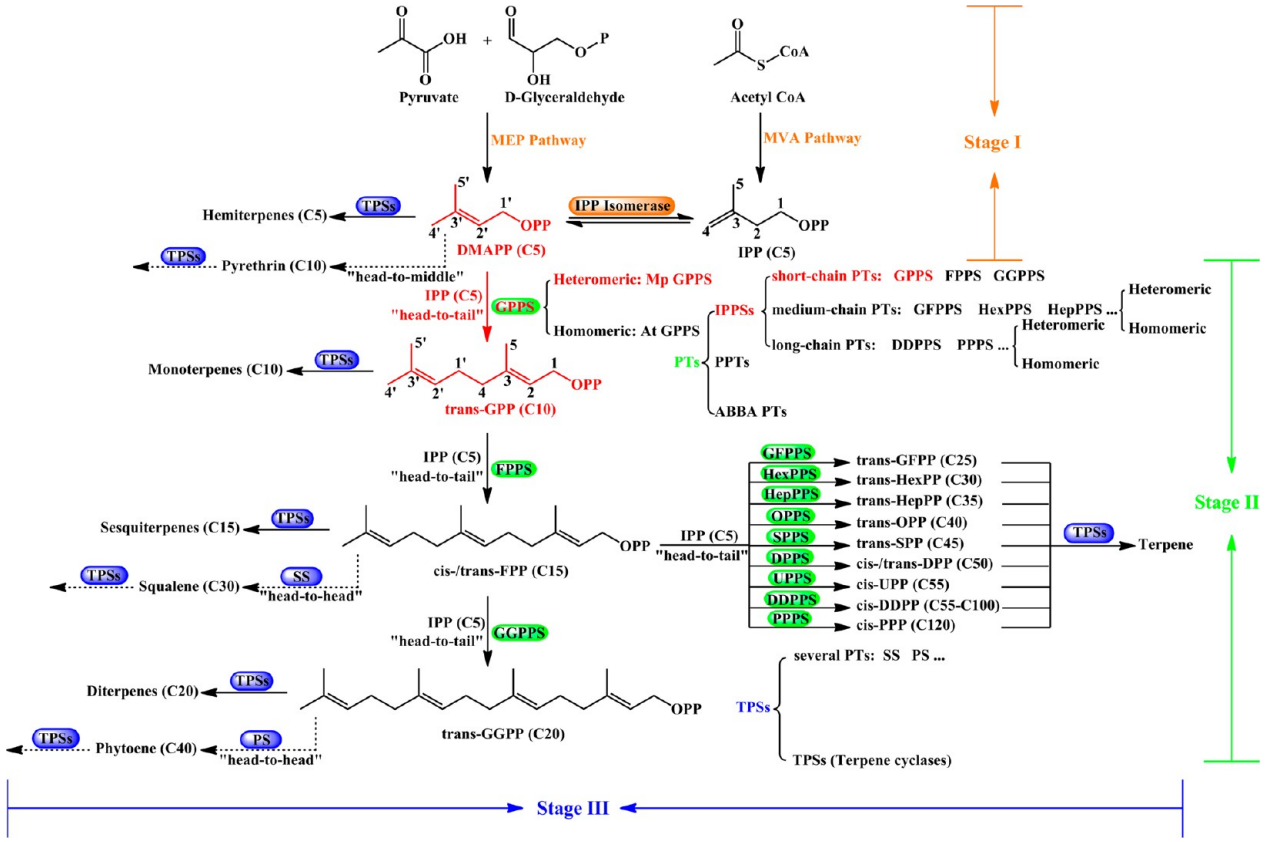

Figure 1. Schematic overview of isoprenoid biosynthesis pathway.

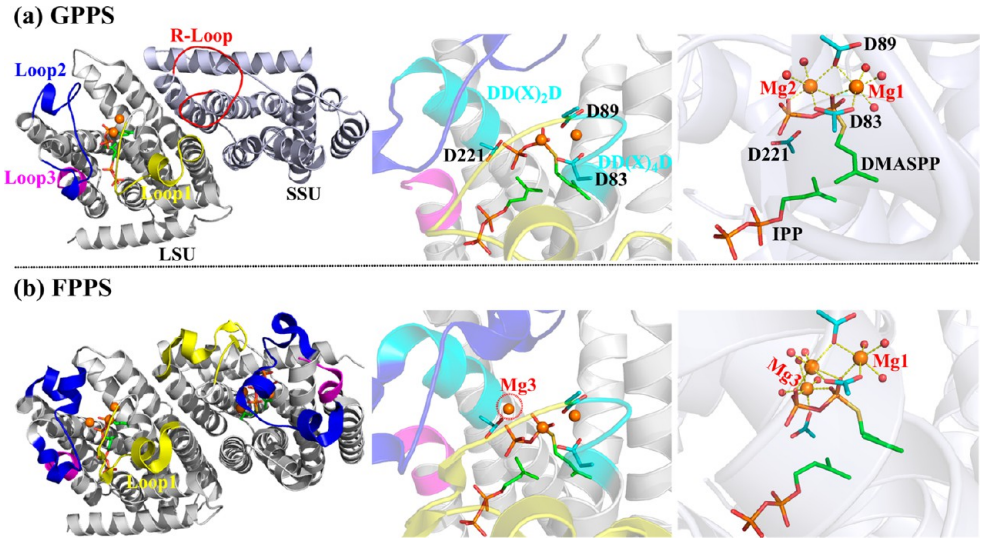

Figure 2. (a) Enzyme−substrate binding mode of GPPS. (b) Enzyme−substrate binding mode of FPPS. Their catalytic cavities are surrounded by three conserved loops denoted as loop1 (in yellow), loop2 (in blue), and loop3 (in pink). Two conserved $DD(X)_{2-4}D$ motifs (where X can be any residues, shown in cyan) are essential for substrate and cofactor binding. The residue ID is based on the *Mp*-GPPS. Herein, the substrate DMAPP is replaced by the substrate analog DMASPP in crystallization.

cyclization,[16,17] and these terpene end products ultimately yield chemically diversified terpenes including various monoterpenes, sesquiterpenes, diterpenes and so forth, catalyzed by the terpene synthases (TPSs) or terpene cyclases.[17,18]

Among the above three stages in the terpene biosynthesis, the chain elongation is the key step and produces terpene precursors for the sequential rearrangement or cyclization.[2,19] As shown in Figure 1, the controller PTs are generally classified into three major groups, namely linear isoprenyl transferases (IPPSs), protein prenyltransferases (PPTs), and aromatic prenyltransferases (ABBA PTs).[4,20] More specifically, the PPTs catalyze the transfer of an isoprenyl pyrophosphate (PPV) to a protein or a peptide,[21,22] and the ABBA PTs catalyze the transfer of prenyl residues to C, O, or N atoms of aromatic structures,[23−25] while the IPPSs catalyze the chain elongation of isoprenoid building block DMAPP via the

DOI: 10.1021/acscatal.5b00947
ACS Catal. 2015, 5, 4466−4478

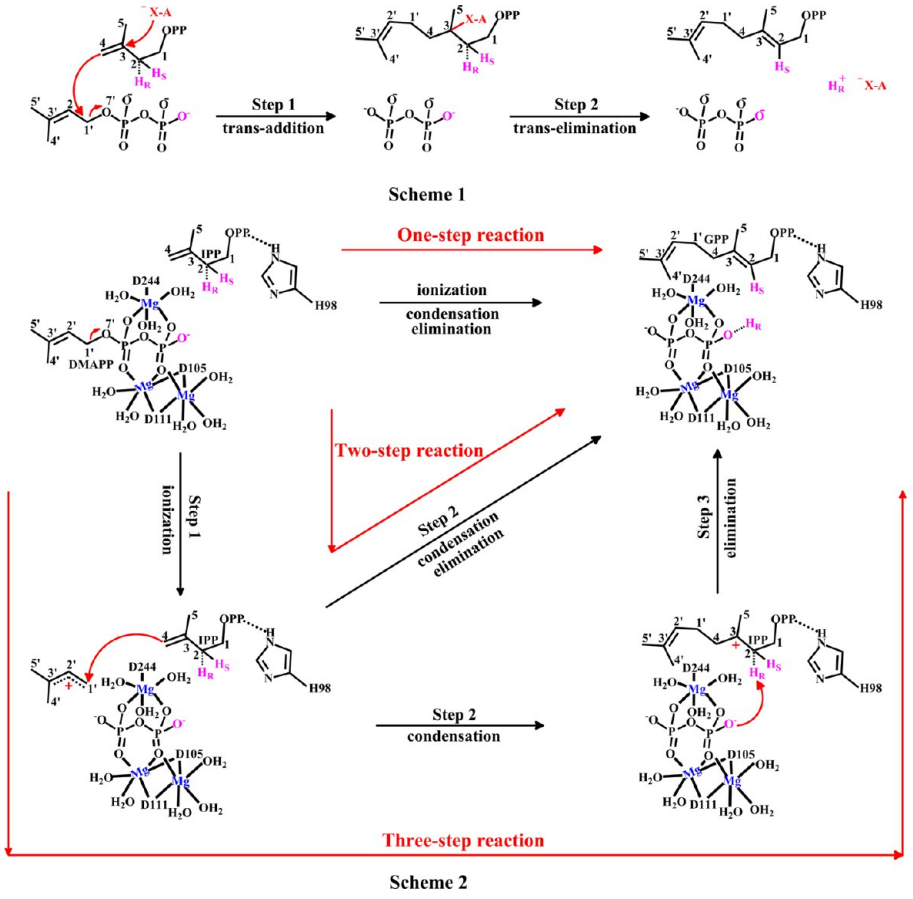

Figure 3. Previously suggested catalytic mechanisms of assembling isoprenoid building blocks for isoprenyl pyrophosphate synthases (IPPSs). Scheme 1: proposed reaction mechanism in a nonenzyme environment. Scheme 2: three possible reaction mechanisms for the coupling of the first C5 units with DMAPP in FPPS. The residue ID is based on the FPPS.

consecutive 1′-4 assembly reactions with IPP to generate linear polymers with defined chain lengths.[19,26] The IPPSs could be further classified into short-chain PTs, medium-chain PTs and long-chain PTs based on the chain lengths of products.[5] The geranyl pyrophosphate synthase (GPPS), which catalyzes the assembly reaction of DMAPP with one IPP to form the geranyl pyrophosphate (GPP, C10),[27−30] and FPPS, which is responsible for the assembly with two IPP to produce the farnesyl pyrophosphate (FPP, C15),[31,32] both fall into the category of short-chain PTs (see Figure 1).[5] Structures of several GPPS and FPPS enzyme-ligand complexes[33,34] have been determined recently. Interestingly, the GPPS family can be divided into homomeric (such as *At*-GPPS) and heteromeric proteins (such as *Mp*-GPPS), while the heteromeric FPPS has not been found or crystallized so far.[4,27−30] Figure 2 shows that the heteromeric *Mp*-GPPS consists of a large subunit (LSU) and a small subunit (SSU) while the homomeric *Ec*-FPPS only include two identical subunits. The catalytic site of LSU is surrounded by three loop motifs denoted as Loop1, Loop2, and Loop3.[33] Loop1 (residues 83−108) contains a $DD(X)_4D$ motif which is highly conserved in the PTs superfamily, Loop2 (residues 220−253) includes a $DD(X)_2D$ motif, and Loop3 (residues 289−295) is thought to be closely related to the IPP binding.[33] Both the active site and $DD(X)_{2-4}D$ motifs are not found in SSU where instead a R-loop is identified and thought to play an important role in the product release.[33,35] These key structural motifs for substrate binding in GPPS were illuminated by our classical molecular dynamics (MD) simulations very recently.[36] As shown in Figure 2, the catalytic site is highly conserved between *Mp*-GPPS and *Ec*-FPPS, and their coordination shells of the center Mg^{2+} ions are highly conserved with the pyrophosphate (PPV) of DMAPP, D83 and D89 in Loop1, D221 in Loop2, and several water molecules. However, a significant difference is that there are three Mg^{2+} ions in the active site of FPPS while only two in GPPS.

A number of structural and computational studies of terpenes have been conducted to explore the molecular basis in the terpene biosynthesis pathway.[37−41] Based on the first crystal structure of *cis*-PTs reported by Fujihashi and co-workers,[42] researchers articulated the enzyme's architecture and the chain elongation mechanism.[26,43] Notably, Tantillo and co-workers performed detailed quantum mechanical dynamics simulations of the terpene formation[44,45] and proposed the reaction mechanism of a triquinane forming sesquiterpene synthase from chamomile by combining computations and deuterium-labeling experiments.[46] Merz et al. explored the substrate selectivity and product regioselectivity of PTs in Orf2[47] as well as the conformational activation of FTase prior to the catalytic reaction.[48] As GPPS is responsible for the critical initial stage of consecutive assemble chain elongation reactions, elucidating its catalytic mechanism is highly important and will help the development of new technology in generating novel natural productlike scaffolds. Unfortunately, there has been no report on the assembly mechanism of DMAPP and IPP catalyzed by GPPS until now. FPPS, as a well-studied and important target for the treatment of parasitic diseases such as Chagas disease

DOI: 10.1021/acscatal.5b00947
ACS Catal. 2015, 5, 4466−4478

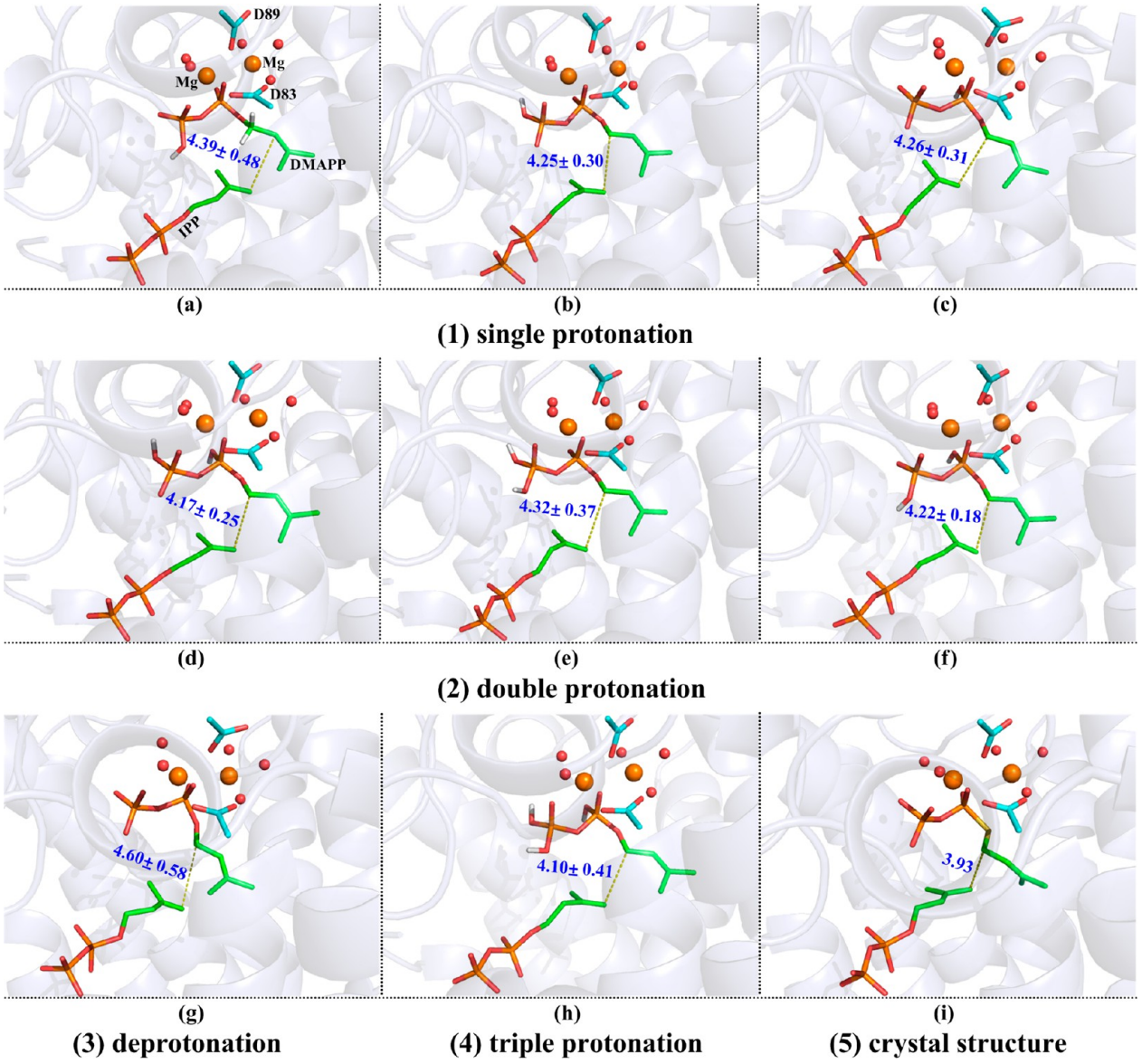

Figure 4. Comparison of keynote distance in GPPS among the XRD structure and various QM/MM-simulated models. (a–c) Three kinds of single protonation models. (d–f) Three kinds of double protonation models. (g) Deprotonation model. (h) Triple protonation model. (i) XRD structure.

and African trypanosomiasis,[49−53] is referential for the mechanistic study of GPPS, since they share similar active site structures as discussed above. Figure 3 summarizes the catalytic mechanisms of IPPS proposed so far. Poulter et al. (Scheme 1 in Figure 3) were the first to suggest the essential "ionization−condensation−elimination" three steps for assembly reactions in 1970s, in which the heterolytic cleavage of the C1′−O7′ bond of DMAPP yields a cationic carbon which subsequently attacks the sp^2 carbon C4 of IPP, and finally a hydrogen atom on C2 of IPP is eliminated to form GPP.[12,13,54,55] Specifically, Cornforth and co-workers confirmed that the last elimination step is the deprotonation of IPP (H_R of C2) based on the nonenzymatic experiment in aqueous solution (Scheme 1 in Figure 3).[56,57] So far, three major reaction mechanisms for FPPS have been proposed (Scheme 2 in Figure 3), and none is widely accepted.[32,34,57,58] The earliest one is the concerted mechanism (namely "one-step reaction"), where the ionization, condensation as well as elimination procedures were assumed to occur synchronously with only one transition state.[56,58] The theoretically predicted reaction barrier is 26.4 kcal/mol with the difference of the C1′−O7′ and C1′−C4 bond distances chosen as the reaction coordinate.[59] Alternatively, the "two-step reaction" mechanism treats the condensation step and the elimination step as concerted.[59−61] The last mechanism is the "three-step reaction" mechanism, where the ionization−condensation−elimination processes are stepwise.[32,34] All of the above three reaction mechanisms concur that the final eliminated proton is H_R but not H_S of IPP, and H_R is then transferred to the PPV cleaved from DMAPP in the first "ionization" reaction.[56]

In this work, Born−Oppenheimer density functional QM/MM molecular dynamics simulations with umbrella sampling, a state-of-the-art approach to simulate enzyme reactions,[62−65] have been performed to characterize the C_S−C_S units (DMAPP and IPP) assembly reaction catalyzed by *Mp*-GPPS. Instead of favoring any of the three existing and controversial mechanisms for FPPS, our computations suggest that the protonation of DMAPP is the key as it triggers the subsequent ionization

DOI: 10.1021/acscatal.5b00947
ACS Catal. 2015, 5, 4466−4478

process. Based on the derived free energy profile along the most probable reaction pathway, the rate-limiting transition state is determined and the catalytic roles of the conserved residues and the two Mg^{2+} ions in the active site are delineated.

2. COMPUTATIONAL METHODS

Similar to our previous classical MD simulations,[36] the crystal structure of *Mp*-GPPS (PDB code: 3KRO)[33] for the heterotetrameric geranyl pyrophosphate synthase (GPPS) from mint (*Mentha piperita*) complexed with the non-hydrolyzable DMAPP analog dimethylallyl thiopyrophosphate (DMASPP) was selected for present study at the QM/MM theoretical level. The spherical boundary condition was applied and the atoms more than 22 Å away from the C1′ atom of DMAPP were fixed. Since the ligands coordinated to metal ions are not involved in the subsequent reaction steps after "ionization", different QM/MM partition schemes were considered for different reaction steps/mechanisms in order to reduce computational costs (see Figure S1). For the ionization step, the QM part is composed of DMAPP, IPP, Asp83, Asp89, Lys180, two Mg^{2+} ions, and five water molecules which coordinate with Mg^{2+} ions. For the condensation and elimination steps, the QM part involves DMAPP, IPP, His76, and Mg^{2+} ions. All the QM subsystems were treated by the density functional theory B3LYP[66,67] with the 6-31+G* basis set for the oxygen atoms of DMAPP/IPP and the 6-31G* basis set for all other atoms. Benchmark tests were performed, as shown in Figure S12 in the Supporting Information. Results confirmed that the theoretical level B3LYP/6-31(+)G* is reliable for this assemble reaction. The QM/MM boundaries were described by the pseudobond approach with the improved pseudobond parameters.[68−71] All remaining atoms were described with the Amber99SB force field at the molecular mechanical (MM) level.[72−74] More detailed description of the computational setups and procedures can be found in the Computational Methods section of the Supporting Information or similarly in our previous computational protocols.[75−79] To track the reaction of assembling isoprenoid building blocks, various combinations of reaction coordinates (RCs) had been chosen (see Figure S2), and all these density functional QM/MM simulations were performed with the modified QChem-Tinker programs.[63,64]

3. RESULTS AND DISCUSSION

3.1. Identification of the Michaelis Complex: The Protonation of DMAPP. As discussed in the above, the high similarity of the active sites in FPPS and GPPS leads to an assumption that the proposed reaction mechanisms of FPPS so far as summarized in Figure 3 apply to GPPS as well. As a consequence, we explored these reaction mechanisms for the assembly of isoprenoid building blocks GPP and IPP by deriving the potential energy profiles along the reaction coordinates defined in Figure S2 for *Mp*-GPPS. However, the resulting energy profiles (Figure S3) show that both the concerted and stepwise mechanisms (where only the first ionization step was studied) are irrational with the original model built in the above section, as the potential energy keeps increasing with reaction barriers higher than 40 kcal/mol. This is in contrast to the case of FPPS, as Sanchez et al. have demonstrated that the reaction barrier (potential energy) for FPPS is only 26.4 kcal/mol.[59]

To find alternative avenues for the chemical assembly catalyzed by GPPS, we compare the present study with two published works. One is related to the farnesyltransferase (FTase).[48] In order to understand how FTase recruits the FPP substrate, Cui and Merz suggested that only when the pyrophosphate (PPV^{3-}) of the FPP is monoprotonated (FPP^{2-}), a stable intermediate state could be identified, in which FTase has a similar active site structure to PTs. In the second work, Jiang et al. demonstrated that the doubly protonated tetrametaphosphate $[P_4O_{12}H_2]^{2-}$ can be easily formed in the methanolysis and protonolysis.[80] These results remind us that the protonation state of DMAPP may be the key point but it is not considered in previous mechanisms for FPPS. Obviously, the protonation of the PPV^{3-} of DMAPP is of great importance on effecting the leaving ability of the PPV group to promote the first "ionization" (i.e., the breakage of C1′-O7′) in view of the basic organic reaction theory. As such, we performed QM/MM MD simulations with all possible protonation states, including one deprotonated model, three singly protonated models, three doubly protonated models and one triply protonated models, in attempt to find the most probable Michaelis complex. Figure 4 shows the stable structures with various protonation states derived from computational simulations, in comparison with the experimental structure. All models favor the C1′−C4 distance around 4 Å, and of particular, the triply protonated Michaelis complex (model g in Figure 4) with the C1′−C4 distance 4.10 ± 0.41 Å is the closest to the crystal structure (3.93 Å). Further structural analysis (see Figure S4) indicates that our QM/MM MD simulations on the triple protonation complex can reproduce the coordination shell of Mg^{2+} and hydrogen bond network around the DMAPP and IPP in the crystal structures.[33]

With these eight models, we performed extensive QM/MM simulations to derive the potential energy profiles for the concerted and stepwise mechanisms. Figure S5 shows that the concerted mechanism for all eight models can be excluded as the potential energy monotonously increases in all cases. For the stepwise mechanism, we examined the first ionization step, and Figure 5 maps out the energy profiles for the eight models.

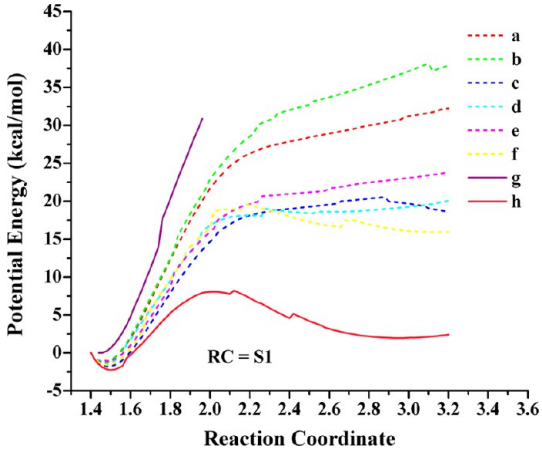

Figure 5. Reaction potential energy curves of the first ionization reaction for GPPS. Herein, a−c and d−f represent the reaction potential energy results of single protonation and double protonation reactant complex, respectively. And, g and h stand for the results of deprotonation and triple protonation reactant complex, respectively. RC refers to Figure S2.

DOI: 10.1021/acscatal.5b00947
ACS Catal. 2015, 5, 4466−4478

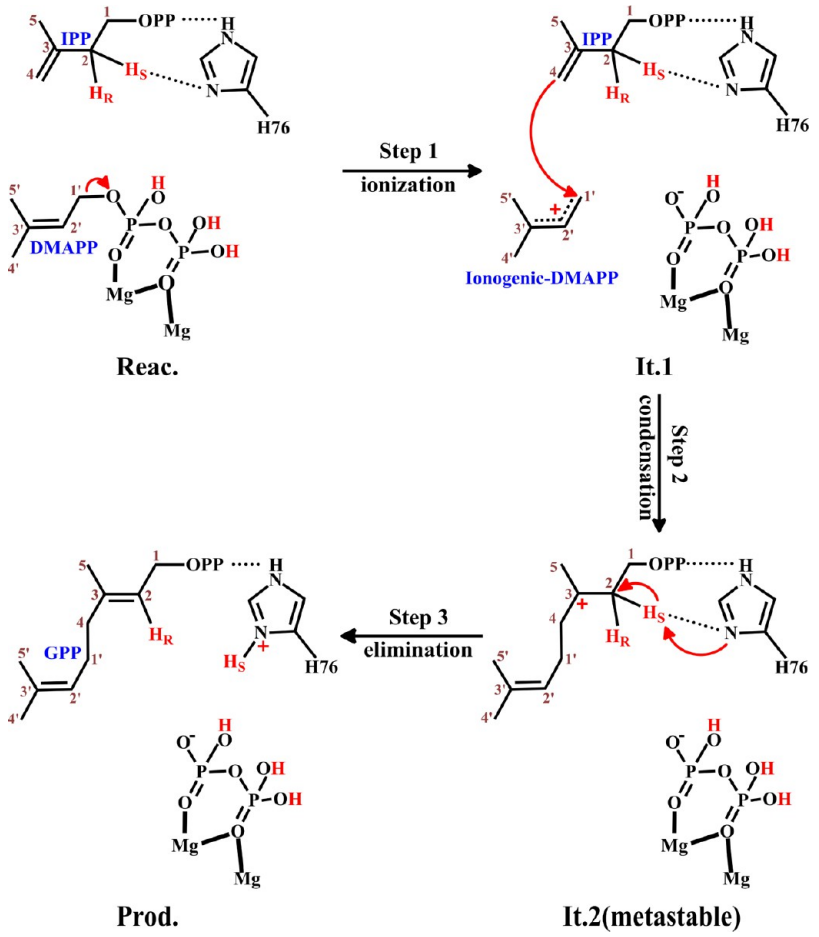

Figure 6. Suggested reaction mechanism of assembling isoprenoid building blocks catalyzed by *Mp*-GPPS from our QM/MM simulations.

Apparently, all singly, doubly protonated and deprotonated models (a–g in Figure 4) are irrational, since there are no distinct transition and intermediate states with these models. The only possibility is the triply protonated model (h in Figure 4), which is the most likely GPPS Michaelis complex, as with this model there is a reaction barrier (~10 kcal/mol) and a metastable intermediate. Further charge analyses (exhibited in Figure S6) show that the electropositivity of C1′ (0.44 vs 0.24) and electronegativity of O7′ (−0.65 vs −0.40) as well as the Lewis acidity of Mg^{2+} (Mg1:1.84 vs 1.24; Mg2:1.86 vs 1.57) are increased with the triple protonation of DMAPP in comparison with the deprotonated state, and thus confirm that the triple protonation of DMAPP is essential to achieve the most likely GPPS Michaelis complex. The rationality of the triply protonated DMAPP is mostly coming from the following two reasons (see detailed discuss in the Supporting Information): One hand, the experimentally measured and computationally predicted p*K*a values indicated that the DMAPP is likely to adopt doubly protonation in the enzyme environment, and the waters in the active pocket could further stabilized the protonated DMAPP via the complicated hydrogen bond network (the binding site/environment of DMAPP is totally different from that of IPP, thus their protonation state is different). The other hand, the further QM/MM calculations show that it is very facile for the proton transfer from K180 to the double-protonated DMAPP to achieve the triple protonation.

In brief, our computational exploration of the most likely initial Michaelis enzyme–substrate complex of GPPS with DMAPP and IPP indicates that DMAPP should be triply protonated on the pyrophosphate group. The following study of the assembly reaction would start from this substrate-triple-protonation Michaelis complex.

3.2. Protonation-Triggered Carbon-Chain Elongation: The Rate-Limiting Elimination Step. As DMAPP is confirmed to be triply protonated, DMAPP will not be able to provide a suitable site to accommodate the H_R proton transferred from IPP in the elimination step. We note that in previously proposed mechanisms for FPPS (see Figure 3) the proton transfer to DMAPP is a necessary step. As such, we propose a different mechanism as shown in Figure 6, where the final elimination step involves the proton transfer (H_s) from IPP to H76: N^{δ}, after the ionization (C1′–O7′ breakage in DMAPP) and condensation (C1′–C4 formation between DMAPP and IPP) steps. Following this mechanism, we performed QM/MM MD simulations to derive the complete free energy profile of the whole assembly reaction catalyzed by GPPS, as shown in Figure 7. Overall, the reaction is exergonic by ~22 kcal/mol, with the free energy activation barrier of 18.8 ± 0.6 kcal/mol. The latter is in agreement with the experimental value of 18.0 kcal/mol estimated from the k_{cat} value of 0.58 ± 0.02 s^{-1}[33] based on the transition state theory, and thus, the reaction rate is mostly controlled by the final elimination step. There are two intermediates identified in our simulations, the first intermediate It1 is stable while the second

DOI: 10.1021/acscatal.5b00947
ACS Catal. 2015, 5, 4466–4478

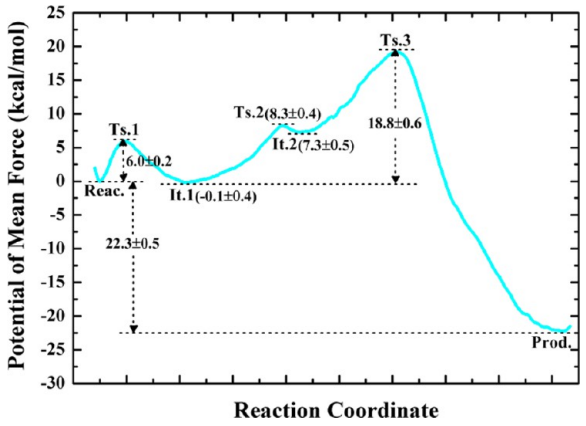

Figure 7. Free energy profile for the assembly reaction catalyzed by *Mp*-GPPS determined by density functional QM/MM MD simulations. The statistical error is estimated by averaging the free energy difference between 5 and 15 ps and 15−25 ps. The chosen reaction coordinates (RC) for each reaction step was illustrated in Figure S2.

one, It.2, is more stable by only 1 kcal/mol than Ts.2, and thus metastable. As the elimination step is proved to be the rate-limiting step, thus the whole reaction is likely undergoing in a stepwise way, and the proposed three-step reaction mechanism is summarized in Figure 6

To better understand the essence of the assembly reaction, we traced the charge evolution of a few selected atoms along the reaction process which is exhibited in Figures 8 and S9. As the PPV of DMAPP is in tight-binding with two Mg^{2+} ions, the high positive charges on the two magnesium cation (∼1.84 e and ∼1.86 e, as shown in Figure 8a) are critical to make the Mg^{2+} ions serve as Lewis acids to polarize the electron density of PPV which would further promote the O7′−C1′ bond breakage. With the ionization step going on, the positive charges on Mg^{2+} ions decrease, e.g., about 1.41 and 1.52 e at Ts.1 and 1.34 and 1.49 e at It.1 (see Figure 8a). These changes suggest that there are certain charge transfers involved intermolecularly in the "ionization" process to immensely stabilize both Ts.1 and It.1, leading to a low reaction energy barrier (∼6 kcal/mol) and a very stable intermediate It.1, since the positive charge removed from Mg^{2+} would be dispersed to the PPV group. Following the C1′−O7′ breakage, the π electrons on the C2′═C3′ double bond would delocalize to the C1′−C2′ single bond intramolecularly, to form a delocalized π bond, and consequently the charge on C1′ decreases from positive (∼0.44 e in Figure 8a) to nearly neutral continually and thus would not yield a carbonium ion after the ionization. Due to the electron delocalization, the bond lengths of C2′−C3′ and C1′−C2′ become very close at It.1, as shown in Figure 8b.

In the "ionization" reaction process, the intramolecular charge transfer within DMAPP is obvious and significant, but the intermolecular charge transfer between DMAPP and IPP as well as the intramolecular charge transfer within IPP are trivial (Figure 8c). The stable negative charge (about −0.6 e with small fluctuations) on C4 atom of IPP remains C4 to serve as a nucleophile, which would promote the subsequent condensation between ionogenic-DMAPP and IPP with the C1′−C4 bond formation. For C1′ atom, its charge increases continually at the beginning of the condensation reaction due to the conformational rearrangement at It.1 state (detailed discussion on the conformation rearrangement of DMAPP and IPP at It.1 state can be found in Figures S7, S8, and S9). Therefore, the condensation occurs between a positively charge carbon and a negatively charged carbon, not between two carbon radicals. Along with the sequential condensation and elimination, the π

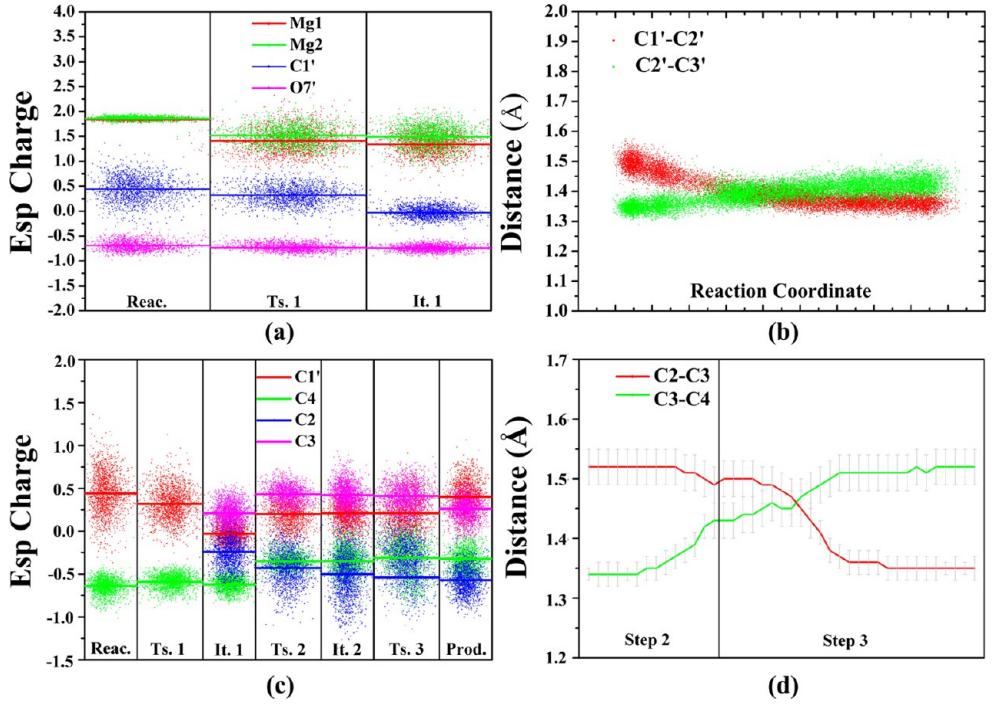

Figure 8. (a) Selected atomic charge variation at the reactant, transition and intermediate states of the first ionization step. (b) Distance variation of C1′−C2′ and C2′−C3′ along the first ionization step. (c) Selected atomic charge variation at the reactant, transition, intermediate, and product states of the whole assembly reaction. (d) Distance variation of C2−C3 and C3−C4 along the second condensation and the third elimination steps.

DOI: 10.1021/acscatal.5b00947
ACS Catal. 2015, 5, 4466−4478

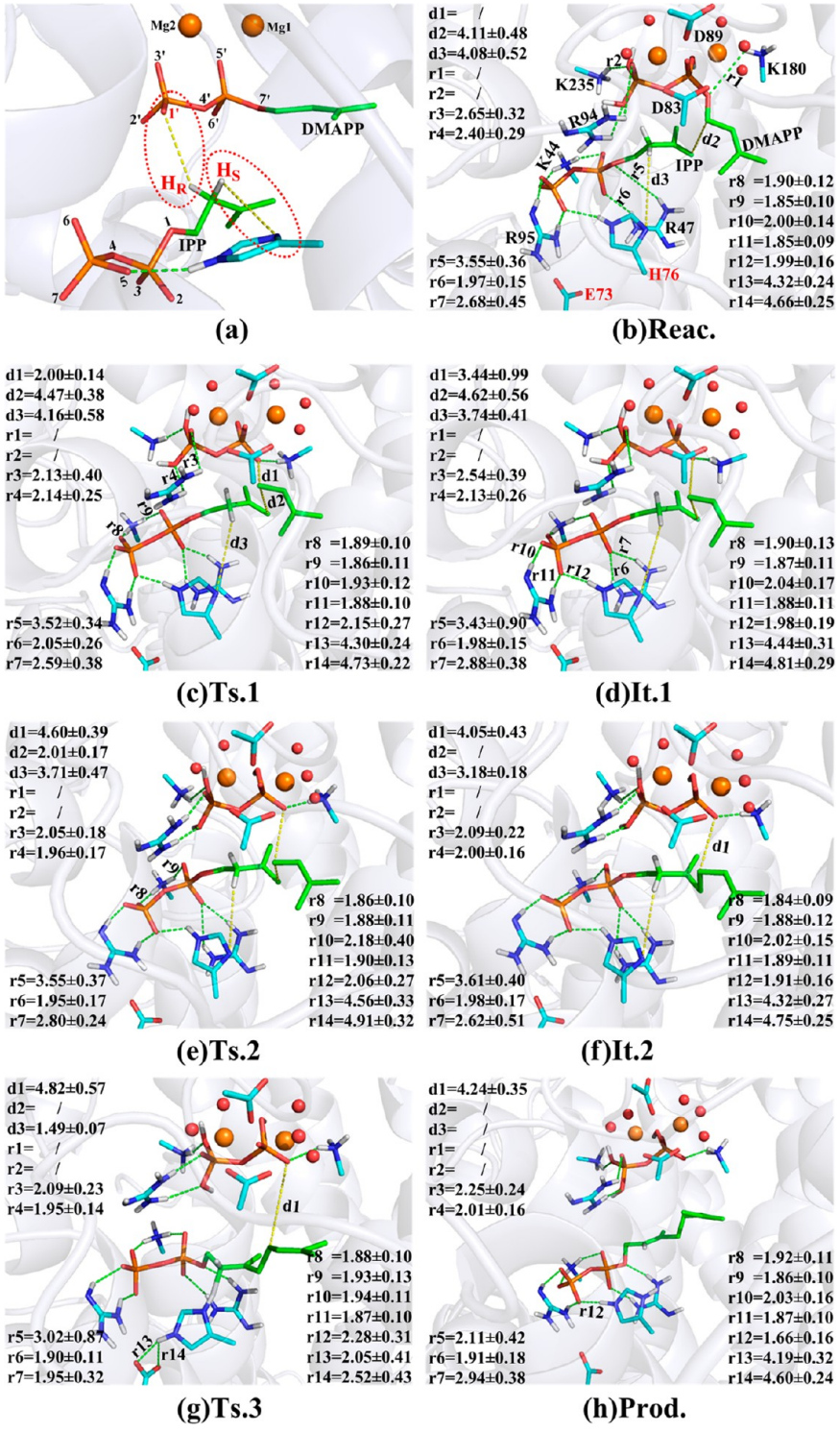

Figure 9. (a) Stereochemistry of the proton elimination in GPPS. (b–h) Active site geometries of the reactant, transition, intermediate, and product states along the assembly reaction in GPPS.

electrons on the C3═C4 double bond delocalize to C1′ intermolecularly and C2 intramolecularly. As a result, the negative charge on C4 reduces to around −0.40 e first and then becomes very stable (about −0.35 e, see Figure 8c), but C3 gets increasingly positive and eventually yields the ionogenic-GPP ($C3^+$). Owing to the elimination of the H_S proton of C2, the charge difference between C2 and C3 is enlarged at the elimination step, and the bond lengths of C2−C3 and C3−C4 gradually reverse, as demonstrated in Figure 8d, and the initial single C2−C3 and double C3═C4 bonds turn to double C2═C3 and single C3−C4 bonds at the end of the elimination step.

Regarding the final elimination step, it was suggested that the H_R on C2 (see Figure 9a) would be abstracted by the leaving PPV of DMAPP based on the earlier work of Cornforth's.[56,57] In our mechanism, however, the H_R proton could not be transferred to PPV of DMAPP since PPV is already triply protonated and there is no suitable site for PPV to accept any proton further. Instead, the neighboring N^{δ} atom of H76 is the

DOI: 10.1021/acscatal.5b00947
ACS Catal. 2015, 5, 4466−4478

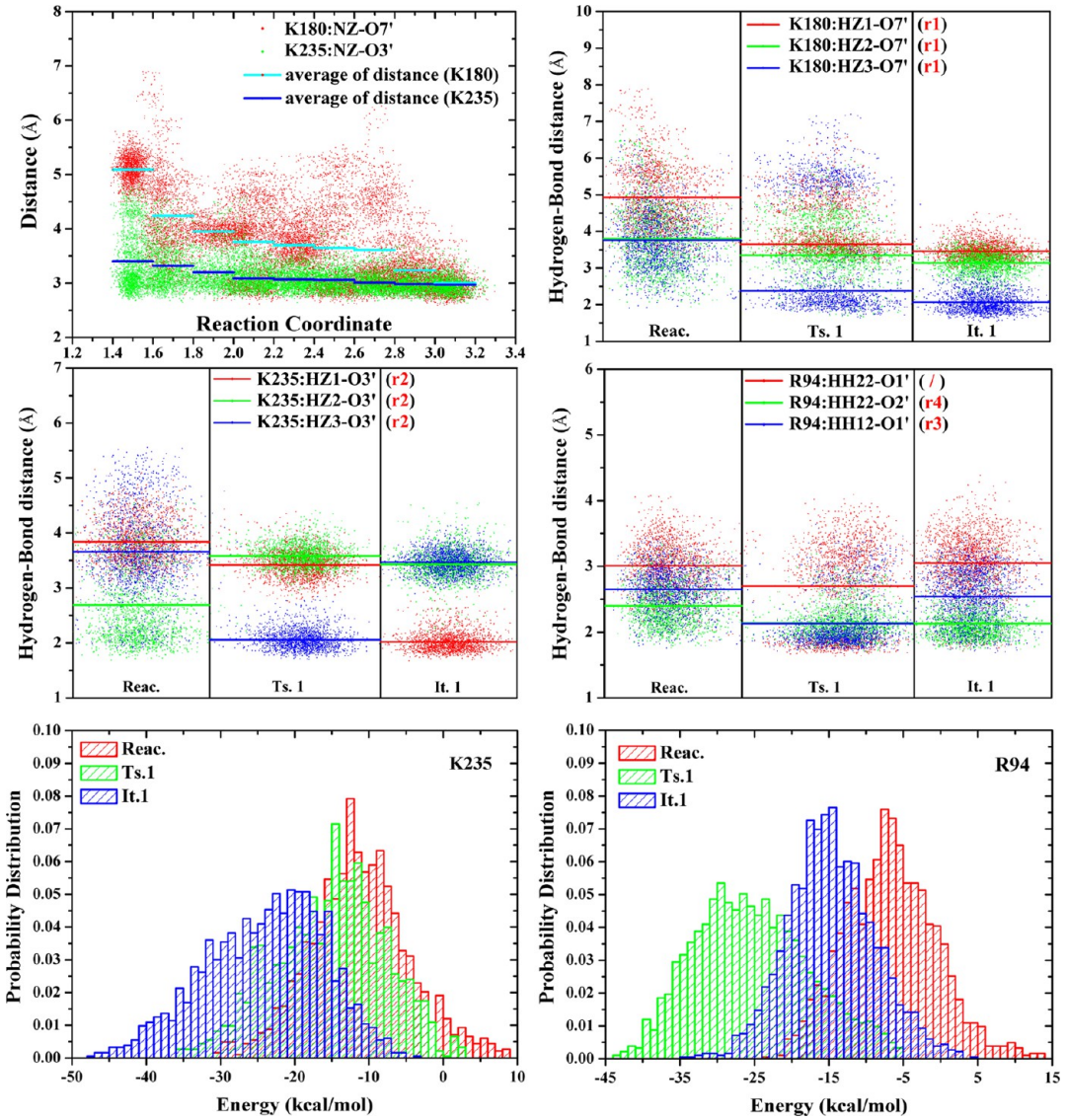

Figure 10. Distance distribution between the selected atoms (upper four pannels) and the interaction energies (electrostatics and van der Waals) distribution between the QM subsystem and key residues (K235 and R94, lower two panels) at the reactant, transition, and intermediate states of the first ionization step. The atom names (HZ1, HZ2, HZ3, HH12, HH22, O1′, O2′, O3′, and O7′) refer to Figure S10, and r1−r4 refer to Figure 9b−h.

possible basic site to accommodate the proton H_S (also on C2) with suitable stereochemical arrangement, as can be seen in Figure 9a. Indeed, the amino acid residue H76 is highly conserved among most IPPSs,[32,33] which implies that H76 might play a nonnegligible role in the assembly reaction. As shown in Figure 9, the distance (d3) between IPP:H_S and H76:N^{δ} gets increasingly short along the ionization and condensation steps. At the It.2 state, d3 is reduced to 3.18 Å. Moreover, a strong hydrogen bond between H76:N^{ε} and PPV of IPP, whose distance r12 is about 1.88 Å, retains along the ionization and condensation reaction. At the beginning of the elimination reaction, double strong hydrogen bonds with E73 will be formed to construct a powerful catalytic dyad, Glu-His dyad (also for Asp-His), which is commonly found to promote proton transfer reaction in many enzymes such as HDACs[81,82] and *Bacillus* subtilis *N*-acetylglucosaminidase.[83]

To experimentally determine the influence of H76 on the GPPS catalytic activity, the H76 amino acid was mutated to an alanine residue (A76), expressed in the *BL21 (DE3)* strains. The finally purified wild type and H76A GPPS were tested for the enzymatic activity via the Pyrophosphate Assay kit (*Fluorometric, Abcam*). The detailed experimental protocol including enzyme expression, purification and activity assay were provided in the Supporting Information, the data and results were summarized in Figures S14−S18 and Table S1. As shown in Table S1 and Figure S18, the enzymatic catalytic activity is almost lost due to H76A mutant (see detailed discussion in Figure S18). It further proves that the H76 is an essential residue and likely directly involves in the enzymatic catalytic chain elongation reaction. To some extent, it indirectly supported our computationally suggested reaction mechanism in which the N^{δ} atom of H76 is the potent basic site to accommodate the proton H_S of IPP in the rate-limiting step.

In summary, our computations suggest that the GPPS-catalyzed assembly reaction is induced by the triple-protonation of DMAPP to generate an ionogenic-DMAPP intermediate (It.1), followed by a metastable intermediate (It.2) which is yielded via the condensation of IPP and ionogenic-DMAPP. Finally, the proton transfer from IPP to H76 overcomes the highest reaction barrier in the whole process to yield the

DOI: 10.1021/acscatal.5b00947
ACS Catal. 2015, 5, 4466−4478

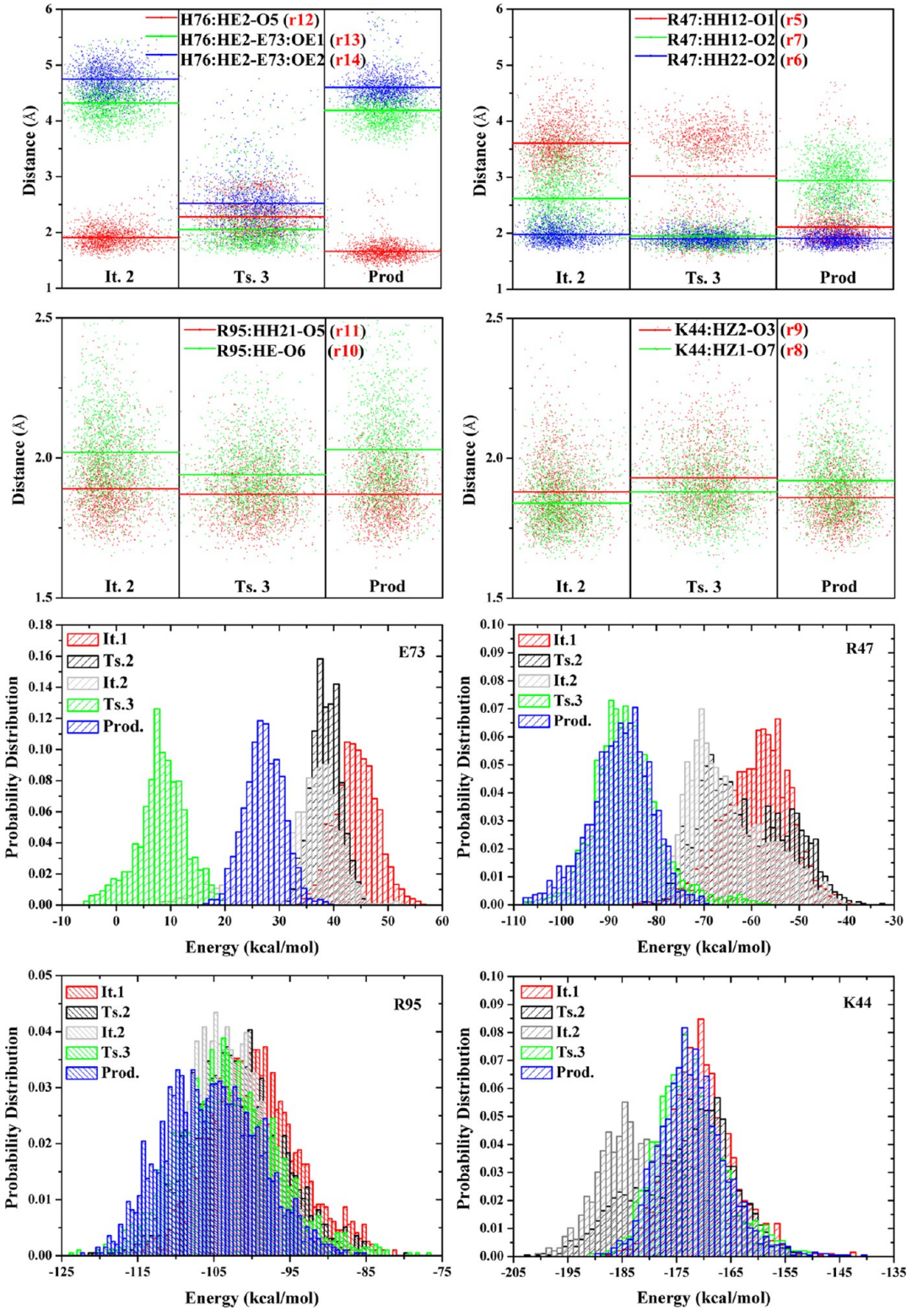

Figure 11. Distance distribution between the selected atoms (upper four panels) and interaction energies (electrostatics and van der Waals) between the QM subsystem and key residues (E73, R47, R95, and K44, lower four panels) at the transition, intermediate, and product states of the second condensation and the third elimination reactions. The atom names (HE2, OE1, OE2, HH12, HH22, HH21, HE, HZ1, HZ2, O1, O2, O3, O5, O6, and O7) refer to Figure S10, and r5−r14 refer to Figure 9b−h.

product GPP, with a large amount of energy released to the surrounding. In this mechanism, only H76 directly participates in the catalysis while all other residues as well as Mg^{2+} ions are not directly involved but also play important environmental roles, which will be discussed in the next section.

3.3. Functional Roles of Key Residues in the Assembly Reaction. We first look at the key residues around DMAPP. Figure 9 shows that K180 and K235 move close to DMAPP along the ionization reaction and form hydrogen bonds via their NH_3^+ groups with O7′ and O3′ respectively. For R94, its

DOI: 10.1021/acscatal.5b00947
ACS Catal. 2015, 5, 4466−4478

interaction with DMAPP gets much stronger at the state Ts.1 with two hydrogen bonds in comparison with the reactant state where there is only one weak hydrogen bond and It.1 which contains one hydrogen bond as well. Further interaction energy analyses, as shown in Figure 10, reveal that both K235 and R94 considerably stabilize the states of It.1 and Ts.1. More specifically, K235 largely stabilizes the intermediate product by about −24.0 kcal/mol, while R94 greatly stabilizes the transition state by about −25.3 kcal/mol.

Around IPP there are a number of residues including E73, R47, R95, K44, and H76. Since IPP is not directly involved in the first ionization step but participates in the final rate-limiting condensation and elimination steps, evolutions of hydrogen bonding and interaction energies are carefully analyzed for the latter two steps, as plotted out in Figure 11 and Figure S11. As E73 is close to the negatively charged PPV of IPP, there is considerable repulsion between E73 and IPP, as evidenced by the energy analyses. But this repulsive interaction is weakened at Ts.3. In other words, the instability of transition state Ts.3 contributed by E73 is reduced, which is beneficial for the following elimination reaction. Differently, there is strong electrostatic attraction between IPP and R47, and the latter thus highly stabilizes both the state Ts.3 and the product state. This stability is consistent with the hydrogen bonding evolution as shown in Figure 11. As for R95 and K44, their strong hydrogen bonds with IPP are maintained well from the state Ts.2 to the product state, and there are little changes for their interaction energies at each reaction state, but R95 is largely responsible for the stabilization of the product state while K44 stabilizes the metastable state It.2.

For H76, the H76···IPP:O5 hydrogen bond becomes weak as the system reaches to the Ts.3 state and then strengthens at the product state. This change is accompanied by the variation of the H76···IPP:O5 hydrogen bond distance which becomes longer from It.2 to Ts.3, and in the meantime, E73 gets close to H76 and finally forms a strong hydrogen-bond with H76 at the state Ts.3. With the presence of this "His-Glu" dyad, H76 acts as a general base to attract the Hs on C2 of DMAPP and then concertedly trigger the formation of carbon−carbon double bond (C2−C3) in IPP to yield the GPP product.

Since the two Mg^{2+} ions are pretty far away from the reaction center in the subsequent rate-determining step, the functional roles of the two Mg^{2+} ions are serving as an anchor to tightly bind DMAPP in the first ionization step. Meanwhile, due to the high positive charges, the Mg^{2+} ions could play as Lewis acids to polarize PPV, and this polarization would also promote the O7′−C1′ bond breakage. Nevertheless, the reactivity is largely triggered by the protonation of DMAPP as discussed in section 3.1.

4. CONCLUSIONS

In this work, the ionization−condensation−elimination assembly mechanism of IPP and DMAPP in *Mp*-GPPS has been investigated by performing extensive Born−Oppenheimer density functional QM/MM MD simulations. We proposed a novel protonation-triggered carbon-chain elongation mechanism, in which the triple protonation of the pyrophosphate (PPV) group of DMAPP is essential for the initial ionization reaction. Besides, the proton transfer in the rate-limiting elimination step occurs from the H_S proton of IPP to the highly conserved residue H76. These two key points are the novelty in our new mechanism which are substantially different from previously hypothesized mechanisms for FPPS. In other words, GPPS seemingly adopts different reaction mechanisms from FPPS. The central Mg^{2+} ions serve as Lewis acids to promote the O7′−C1′ bond breakage in the ionization process, while H76 acts as a general base to attract the Hs on C2 of DMAPP in the elimination procedure. Moreover, further mutant experiments confirm that the H76 is an essential residue and likely directly involving in the rate-limiting step of enzymatic catalysis. For the ionization reaction, K235 mostly stabilizes the intermediate product while R94 is responsible for the stabilization of the transition state. In the condensation and elimination steps, R95 contributes to the stabilization of the product state, K44 stabilizes the metastable intermediate, and R47 profoundly stabilizes both the transition state and product state. All the detailed information on the structural and functional changes of various residues provides insight into the reaction mechanism in *Mp*-GPPS and is helpful for the potential biosynthesis of novel natural productlike molecular scaffolds which are crucial in the drug lead identification process and also referential for FPPS inhibitor design.

■ ASSOCIATED CONTENT

Supporting Information

The Supporting Information is available free of charge on the ACS Publications website at DOI: 10.1021/acscatal.5b00947.

Computational methods; rationality of triple protonated DMAPP; experimental methods; references; Ddetailed QM/MM partition schemes; illustration of the reaction coordinate (RC); illustration of the potential energy curves along the different reaction coordinates; comparison of the binding pocket in the XRD, MM MD, and QM/MM MD simulations; charge analysis distance variations for the selected atoms/residues; conformation rearrangement of IPP and DMAPP around state It.1; benchmark test on the M06-2X vs B3LYP methods with various basis-set; the wild type and mutant protein expression, purification and enzymatic activity experiments. (PDF)

■ AUTHOR INFORMATION

Corresponding Authors

*E-mail: wurb3@mail.sysu.edu.cn (R.W.).
*E-mail: yirong.mo@wmich.edu (Y.M.).

Notes

The authors declare no competing financial interest.

■ ACKNOWLEDGMENTS

This work was supported by the National Science foundation of China (21203257 and 21272289) and Pearl River S&T Nova Program of Guangzhou (2014J2200062). H.-B.L. would like to thank the NSFC for support (21103234). We thank the National Supercomputing Centers in Shenzhen and Guangzhou for providing the computational resources. We also thank Prof. Yingkai Zhang and Dr. Shenglong Wang at NYU for their help in using QChem-Tinker.

■ REFERENCES

(1) Gershenzon, J.; Dudareva, N. *Nat. Chem. Biol.* **2007**, *3*, 408−414.
(2) Vandermoten, S.; Santini, S.; Haubruge, E.; Heuze, F.; Francis, F.; Brasseur, R.; Cusson, M.; Charloteaux, B. *Insect Biochem. Mol. Biol.* **2009**, *39*, 707−716.
(3) Oldfield, E.; Lin, F. Y. *Angew. Chem., Int. Ed.* **2012**, *51*, 1124−1137.

DOI: 10.1021/acscatal.5b00947
ACS Catal. 2015, 5, 4466−4478

(4) Kumari, S.; Priya, P.; Misra, G.; Yadav, G. *Phytochem. Rev.* **2013**, *12*, 255−291.
(5) Vandermoten, S.; Haubruge, E.; Cusson, M. *Cell. Mol. Life Sci.* **2009**, *66*, 3685−3695.
(6) Gao, Y.; Honzatko, R. B.; Peters, R. J. *Nat. Prod. Rep.* **2012**, *29*, 1153−1175.
(7) Bouvier, F.; Rahier, A.; Camara, B. *Prog. Lipid Res.* **2005**, *44*, 357−429.
(8) Miziorko, H. M. *Arch. Biochem. Biophys.* **2011**, *505*, 131−143.
(9) Korman, T. P.; Sahachartsiri, B.; Li, D.; Vinokur, J. M.; Eisenberg, D.; Bowie, J. U. *Protein Sci.* **2014**, *23*, 576−585.
(10) Vinokur, J. M.; Korman, T. P.; Cao, Z.; Bowie, J. U. *Biochemistry* **2014**, *53*, 4161−4168.
(11) Rohmer, M. *Lipids* **2008**, *43*, 1095−1107.
(12) Kellogg, B. A.; Poulter, C. D. *Curr. Opin. Chem. Biol.* **1997**, *1*, 570−578.
(13) Ogura, K.; Koyama, T. *Chem. Rev.* **1998**, *98*, 1263−1276.
(14) Vranova, E.; Coman, D.; Gruissem, W. *Mol. Plant* **2012**, *5*, 318−333.
(15) Martin, D. M. *Plant Physiol.* **2003**, *132*, 1586−1599.
(16) Brandt, W.; Brauer, L.; Gunnewich, N.; Kufka, J.; Rausch, F.; Schulze, D.; Schulze, E.; Weber, R.; Zakharova, S.; Wessjohann, L. *Phytochemistry* **2009**, *70*, 1758−1775.
(17) Lange, B. M.; Ghassemian, M. *Plant Mol. Biol.* **2003**, *51*, 925−948.
(18) Wendt, K. U.; Schulz, G. E. *Structure* **1998**, *6*, 127−133.
(19) Kloer, D. P.; Welsch, R.; Beyer, P.; Schulz, G. E. *Biochemistry* **2006**, *45*, 15197−15204.
(20) Liang, P. H.; Ko, T. P.; Wang, A. H. J. *Eur. J. Biochem.* **2002**, *269*, 3339−3354.
(21) Casey, P. J.; Seabra, M. C. *J. Biol. Chem.* **1996**, *271*, 5289−5292.
(22) Wiemer, A. J.; Hohl, R. J.; Wiemer, D. F. *Anticancer Agents Med. Chem.* **2009**, *9*, 526−542.
(23) Saleh, O.; Haagen, Y.; Seeger, K.; Heide, L. *Phytochemistry* **2009**, *70*, 1728−1738.
(24) Tello, M.; Kuzuyama, T.; Heide, L.; Noel, J. P.; Richard, S. B. *Cell. Mol. Life Sci.* **2008**, *65*, 1459−1463.
(25) Botta, B.; Delle Monache, G.; Menendez, P.; Boffi, A. *Trends Pharmacol. Sci.* **2005**, *26*, 606−608.
(26) Liang, P. H. *Biochemistry* **2009**, *48*, 6562−6570.
(27) Burke, C. C.; Wildung, M. R.; Croteau, R. *Proc. Natl. Acad. Sci. U. S. A.* **1999**, *96*, 13062−13067.
(28) Burke, C.; Croteau, R. *Arch. Biochem. Biophys.* **2002**, *405*, 130−136.
(29) van Schie, C. C. N.; Ament, K.; Schmidt, A.; Lange, T.; Haring, M. A.; Schuurink, R. C. *Plant J.* **2007**, *52*, 752−762.
(30) Kang, J. H.; Gonzales-Vigil, E.; Matsuba, Y.; Pichersky, E.; Barry, C. S. *Plant Physiol.* **2014**, *164*, 80−91.
(31) Koyama, T.; Tajima, M.; Sano, H.; Doi, T.; Koike-Takeshita, A.; Obata, S.; Nishino, T.; Ogura, K. *Biochemistry* **1996**, *35*, 9533−9538.
(32) Gabelli, S. B.; McLellan, J. S.; Montalvetti, A.; Oldfield, E.; Docampo, R.; Amzel, L. M. *Proteins: Struct., Funct., Genet.* **2006**, *62*, 80−88.
(33) Chang, T. H.; Hsieh, F. L.; Ko, T. P.; Teng, K. H.; Liang, P. H.; Wang, A. H. *Plant Cell* **2010**, *22*, 454−467.
(34) Hosfield, D. J.; Zhang, Y.; Dougan, D. R.; Broun, A.; Tari, L. W.; Swanson, R. V.; Finn, J. *J. Biol. Chem.* **2004**, *279*, 8526−8529.
(35) Hsieh, F. L.; Chang, T. H.; Ko, T. P.; Wang, A. H. *J. Mol. Biol.* **2010**, *404*, 859−873.
(36) Liu, Z. H.; Zhou, J. W.; Wu, R. B.; Xu, J. *J. Chem. Theory Comput.* **2014**, *10*, 5057−5067.
(37) Major, D. T.; Freud, Y.; Weitman, M. *Curr. Opin. Chem. Biol.* **2014**, *21C*, 25−33.
(38) Major, D. T.; Weitman, M. *J. Am. Chem. Soc.* **2012**, *134*, 19454−19462.
(39) Rajamani, R.; Gao, J. *J. Am. Chem. Soc.* **2003**, *125*, 12768−12781.
(40) van der Kamp, M. W.; Mulholland, A. J. *Biochemistry* **2013**, *52*, 2708−2728.
(41) van der Kamp, M. W.; Sirirak, J.; Zurek, J.; Allemann, R. K.; Mulholland, A. J. *Biochemistry* **2013**, *52*, 8094−8105.
(42) Fujihashi, M.; Zhang, Y. W.; Higuchi, Y.; Li, X. Y.; Koyama, T.; Miki, K. *Proc. Natl. Acad. Sci. U. S. A.* **2001**, *98*, 4337−4342.
(43) Kharel, Y.; Koyama, T. *Nat. Prod. Rep.* **2003**, *20*, 111−118.
(44) Pemberton, R. P.; Tantillo, D. J. *Chem. Sci.* **2014**, *5*, 3301−3308.
(45) Tantillo, D. J. *Nat. Prod. Rep.* **2011**, *28*, 1035−1053.
(46) Hong, Y. J.; Irmisch, S.; Wang, S. C.; Garms, S.; Gershenzon, J.; Zu, L. S.; Kollner, T. G.; Tantillo, D. J. *Chem. - Eur. J.* **2013**, *19*, 13590−13600.
(47) Cui, G.; Li, X.; Merz, K. M., Jr. *Biochemistry* **2007**, *46*, 1303−1311.
(48) Cui, G.; Merz, K. M., Jr. *Biochemistry* **2007**, *46*, 12375−12381.
(49) Ling, Y.; Sahota, G.; Odeh, S.; Chan, J. M.; Araujo, F. G.; Moreno, S. N.; Oldfield, E. *J. Med. Chem.* **2005**, *48*, 3130−3140.
(50) Cinque, G. M.; Szajnman, S. H.; Zhong, L.; Docampo, R.; Schvartzapel, A. J.; Rodriguez, J. B.; Gros, E. G. *J. Med. Chem.* **1998**, *41*, 1540−1554.
(51) Garzoni, L. R.; Waghabi, M. C.; Baptista, M. M.; de Castro, S. L.; Meirelles, M. N.; Britto, C. C.; Docampo, R.; Oldfield, E.; Urbina, J. A. *Int. J. Antimicrob. Agents* **2004**, *23*, 286−290.
(52) Garzoni, L. R.; Caldera, A.; Meirelles, M. N.; de Castro, S. L.; Docampo, R.; Meints, G. A.; Oldfield, E.; Urbina, J. A. *Int. J. Antimicrob. Agents* **2004**, *23*, 273−285.
(53) Montalvetti, A.; Bailey, B. N.; Martin, M. B.; Severin, G. W.; Oldfield, E.; Docampo, R. *J. Biol. Chem.* **2001**, *276*, 33930−33937.
(54) Poulter, C. D.; Satterwhite, D. M. *Biochemistry* **1977**, *16*, 5470−5478.
(55) Poulter, D. C.; Rilling, H. C. *Acc. Chem. Res.* **1978**, *11*, 307−313.
(56) Cornforth, J. W.; Cornforth, R. H.; Popjak, G.; Yengoyan, L. *J. Biol. Chem.* **1966**, *241*, 3970−3987.
(57) Cornforth, J. W. *Angew. Chem., Int. Ed. Engl.* **1968**, *7*, 903−911.
(58) Rilling, H. C.; Bloch, K. *J. Biol. Chem.* **1959**, *234*, 1424−1432.
(59) Sanchez, V. M.; Crespo, A.; Gutkind, J. S.; Turjanski, A. G. *J. Phys. Chem. B* **2006**, *110*, 18052−18057.
(60) Tarshis, L. C.; Yan, M.; Poulter, C. D.; Sacchettini, J. C. *Biochemistry* **1994**, *33*, 10871−10877.
(61) Martin, M. B.; Arnold, W.; Heath, H. T.; Urbina, J. A.; Oldfield, E. *Biochem. Biophys. Res. Commun.* **1999**, *263*, 754−758.
(62) Torrie, G. M.; Valleau, J. P. *J. Comput. Phys.* **1977**, *23*, 187−199.
(63) Ponder, J. W. *TINKER, Software Tools for Molecular Design*, Version 4.2; Washington University School of Medicine: St. Louis, MO, 2004.
(64) Shao, Y.; Fusti-Molnar, L.; Jung, Y.; Kussmann, J.; Ochsenfeld, C.; Brown, S. T.; Gilbert, A. T.; Slipchenko, L. V.; Levchenko, S. V.; O'Neill, D. P.; DiStasio, R. A.; Lochan, R. C.; Wang, T.; Beran, G. J.; Besley, N. A.; Herbert, J. M.; Lin, C. Y.; Van Voorhis, T.; Chien, S. H.; Sodt, A.; Steele, R. P.; Rassolov, V. A.; Maslen, P. E.; Korambath, P. P.; Adamson, R. D.; Austin, B.; Baker, J.; Byrd, E. F.; Dachsel, H.; Doerksen, R. J.; Dreuw, A.; Dunietz, B. D.; Dutoi, A. D.; Furlani, T. R.; Gwaltney, S. R.; Heyden, A.; Hirata, S.; Hsu, C. P.; Kedziora, G.; Khalliulin, R. Z.; Klunzinger, P.; Lee, A. M.; Lee, M. S.; Liang, W.; Lotan, I.; Nair, N.; Peters, B.; Proynov, E. I.; Pieniazek, P. A.; Rhee, Y. M.; Ritchie, J.; Rosta, E.; Sherrill, C. D.; Simmonett, A. C.; Subotnik, J. E.; Woodcock, H. L.; Zhang, W.; Bell, A. T.; Chakraborty, A. K.; Chipman, D. M.; Keil, F. J.; Warshel, A.; Hehre, W. J.; Schaefer, H. F.; Kong, J.; Krylov, A. I.; Gill, P. M.; Head-Gordon, M. *Phys. Chem. Chem. Phys.* **2006**, *8*, 3172−3191.
(65) Vijayaraj, R.; Van Damme, S.; Bultinck, P.; Subramanian, V. *J. Phys. Chem. B* **2012**, *116*, 9922−9933.
(66) Becke, A. D. *Phys. Rev. A: At., Mol., Opt. Phys.* **1988**, *38*, 3098−3100.
(67) Lee, C.; Yang, W.; Parr, R. G. *Phys. Rev. B: Condens. Matter Mater. Phys.* **1988**, *37*, 785−789.
(68) Zhang, Y. K.; Liu, H. Y.; Yang, W. T. *J. Chem. Phys.* **2000**, *112*, 3483−3492.
(69) Zhang, Y. K. *J. Chem. Phys.* **2005**, *122*, 024114−1−024114−7.
(70) Zhang, Y. K. *Theor. Chem. Acc.* **2006**, *116*, 43−50.

DOI: 10.1021/acscatal.5b00947
ACS Catal. 2015, 5, 4466−4478

(71) Zhang, Y. K.; Lee, T. S.; Yang, W. T. *J. Chem. Phys.* **1999**, *110*, 46−54.
(72) Cornell, W. D.; Cieplak, P.; Bayly, C. I.; Gould, I. R.; Merz, K. M.; Ferguson, D. M.; Spellmeyer, D. C.; Fox, T.; Caldwell, J. W.; Kollman, P. A. *J. Am. Chem. Soc.* **1995**, *117*, 5179−5197.
(73) Wang, J. M.; Cieplak, P.; Kollman, P. A. *J. Comput. Chem.* **2000**, *21*, 1049−1074.
(74) Hornak, V.; Abel, R.; Okur, A.; Strockbine, B.; Roitberg, A.; Simmerling, C. *Proteins: Struct., Funct., Genet.* **2006**, *65*, 712−725.
(75) Wu, R. B.; Wang, S. L.; Zhou, N. J.; Cao, Z. X.; Zhang, Y. K. *J. Am. Chem. Soc.* **2010**, *132*, 9471−9479.
(76) Wu, R. B.; Lu, Z. Y.; Cao, Z. X.; Zhang, Y. K. *J. Am. Chem. Soc.* **2011**, *133*, 6110−6113.
(77) Wu, R. B.; Gong, W. J.; Liu, T.; Zhang, Y. K.; Cao, Z. X. *J. Phys. Chem. B* **2012**, *116*, 1984−1991.
(78) Wu, R. B.; Hu, P.; Wang, S. L.; Cao, Z. X.; Zhang, Y. K. *J. Chem. Theory Comput.* **2010**, *6*, 337−343.
(79) Chen, N. H.; Zhou, J. W.; Li, J. B.; Xu, J.; Wu, R. B. *J. Chem. Theory Comput.* **2014**, *10*, 1109−1120.
(80) Jiang, Y.; Chakarawet, K.; Kohout, A. L.; Nava, M.; Marino, N.; Cummins, C. C. *J. Am. Chem. Soc.* **2014**, *136*, 11894−11897.
(81) Pavletich, N. P.; Donigian, J. R.; Cohen, A.; Richon, V. M.; Rifkind, R. A.; Marks, P. A.; Breslow, R.; Finnin, M. S. *Nature* **1999**, *401*, 188−193.
(82) Nielsen, T. K.; Hildmann, C.; Dickmanns, A.; Schwienhorst, A.; Ficner, R. *J. Mol. Biol.* **2005**, *354*, 107−120.
(83) Litzinger, S.; Fischer, S.; Polzer, P.; Diederichs, K.; Welte, W.; Mayer, C. *J. Biol. Chem.* **2010**, *285*, 35675−35684.

DOI: 10.1021/acscatal.5b00947
ACS Catal. 2015, 5, 4466−4478